



This is a repository copy of *Electromagnetic and thermal behavior of a triple redundant 9-phase PMASynRM with insulation deterioration fault*.

White Rose Research Online URL for this paper:
<https://eprints.whiterose.ac.uk/164867/>

Version: Accepted Version

Article:

Shi, Y., Wang, J. orcid.org/0000-0003-4870-3744, Hu, R. et al. (1 more author) (2020) Electromagnetic and thermal behavior of a triple redundant 9-phase PMASynRM with insulation deterioration fault. *IEEE Transactions on Industry Applications*, 56 (6). pp. 6374-6383. ISSN 0093-9994

<https://doi.org/10.1109/tia.2020.3014274>

© 2020 IEEE. Personal use of this material is permitted. Permission from IEEE must be obtained for all other users, including reprinting/ republishing this material for advertising or promotional purposes, creating new collective works for resale or redistribution to servers or lists, or reuse of any copyrighted components of this work in other works. Reproduced in accordance with the publisher's self-archiving policy.

Reuse

Items deposited in White Rose Research Online are protected by copyright, with all rights reserved unless indicated otherwise. They may be downloaded and/or printed for private study, or other acts as permitted by national copyright laws. The publisher or other rights holders may allow further reproduction and re-use of the full text version. This is indicated by the licence information on the White Rose Research Online record for the item.

Takedown

If you consider content in White Rose Research Online to be in breach of UK law, please notify us by emailing eprints@whiterose.ac.uk including the URL of the record and the reason for the withdrawal request.



eprints@whiterose.ac.uk
<https://eprints.whiterose.ac.uk/>

Electromagnetic and thermal behavior of a triple redundant 9-phase PMASynRM with insulation deterioration fault

Yanwen Shi, Jiabin Wang, Senior Member, *IEEE*, Rongguang Hu, and Bo Wang, Member, *IEEE*.
Department of Electronic and Electrical Engineering, The University of Sheffield, UK

Abstract— This paper analyzes the electromagnetic and thermal behavior when insulation deteriorates, leading to short circuit faults in a triple redundant 9-phase permanent magnet assisted synchronous reluctance machine (PMASynRM). It defines a critical insulation resistance at which the temperature in the faulted insulation region reaches the cut-through temperature of the insulation material and determines the minimum and maximum bounds of the critical resistance for all possible faulty insulation volumes by 3D thermal analysis. It suggests insulation resistance thresholds for fault detection and mitigation action in order to prevent complete insulation failure with serious consequences. Moreover, an example is given to show that the insulation deterioration process may begin from large insulation resistance and is accelerated when the insulation material resistivity decreases with increase in temperature. Finally, tests on a prototype machine drive are performed to validate the predicted electromagnetic behavior under turn-to-turn insulation deterioration leading to SC faults.

Index Terms— Permanent magnet-assisted synchronous reluctance motor, insulation deterioration, 3D thermal model, detection threshold.

I. INTRODUCTION

Since the stator winding failure is the second major faults in electrical machines [1-2], quality of winding insulation is key to the reliability of electrical machines in safety critical applications, such as “All Electric Aircraft” and “More Electric Aircraft” (MEA). The winding insulation in electrical machines suffered from combined thermal, electrical, mechanical, and environmental stresses during operation [3]. These stresses result in deterioration of winding insulation and may even lead to short-circuit (SC) faults.

Many published papers have studied machine performance under ideal SC fault conditions assuming that the electric resistance of the insulation becomes zero [4-6]. The work described in [4] investigates the effect of the number of SC turns on SC current and shows that a single-turn SC fault leads to the lowest impedance of the faulty circuit path, resulting in the highest fault current. From this, it can be deduced that a SC fault of one entire phase is less severe. Based on this understanding, most fault detection and mitigation measures reported in literature are tested and validated under the ideal one turn or a few turns SC [5-6]. The temperature distribution, especially the hotspot temperature, under one turn SC, when the

mitigation measure of 3-phase terminal SC which significantly reduces the turn SC current is applied, has been analyzed to ensure fault tolerant ability in terms of thermal behavior [7].

However, in reality when the insulation material degrades, the insulation resistance changes in a few orders of magnitude through a complex process, from a few tens/hundreds of Mega ohms in healthy condition to a few hundred ohms before reaching the ideal SC condition (zero resistance). Meanwhile, most papers reviewed in [3, 8, 9] only focus on qualitative evaluations of the thermal ageing behavior of the insulation for assessing the lifetime of the insulation system. The damage risks of the machine resulting from large current and loss due to aging insulation before reaching the ideal SC condition are seldom considered. Lack of this knowledge may lead to inappropriate requirements and specifications for fault detection methods and mitigation measures.

It should be note that fault detection and mitigation is indispensable for fault tolerant drives. The fault detection must respond quickly and accurately for application of appropriate mitigation measure to prevent fault propagation before causing further damage to the drive system [10]. Therefore, it is essential to have the understanding of the characteristics during insulation deterioration for achieving a reliable fault detection and mitigation measure, and a high level of fault tolerance [11].

This paper will analyze the electromagnetic (EM) and thermal behavior under insulation deterioration leading to SC faults of a triple redundant 9-phase PMASynRM [11]. In addition, it will quantify the range of the cut-through resistance, which is defined as the minimum resistance before irreversible damage of insulation due to heating would take place, for all possible faulty insulation volumes by 3D thermal modelling under turn-to-turn insulation deterioration leading to SC faults. Further, the insulation resistance thresholds for fault detection and mitigation to prevent the catastrophic failure have been given. An example with particular insulation volume has been analyzed with a 3D thermal model to show the aging process when the electrical resistance decreases with increase in temperature. Tests are performed to validate the predicted EM behavior under turn-to-turn insulation deterioration leading to SC faults.

II. EM BEHAVIOR UNDER INSULATION DETERIORATION LEADING TO SC FAULTS

A. 9-phase (3x3-phase) PMASynRM

A triple redundant, 9-phase (3x3-phase), 36-slot, 6-pole PMASynRM as shown in Fig. 1 is reported in [12] for MEA application. The machine employs single layer winding with 2 series connected coils per phase and each coil has 8 turns. This machine employs three separated 3-phase windings denoted as ABC, DEF and GHI. Each forms a balanced 3-phase winding that does not overlap with the other 3-phase sets. Three standard 3-phase inverters are used to drive each 3-phase set. Thus, fault propagation between different 3-phase winding sets is minimized. These together with the low permanent magnet usage largely improve the fault tolerance under many common faults [13-14]. Moreover, it has been demonstrated in [13] that the machine drive can sustain and tolerate a single turn SC fault in the leading or trailing coils of a 3-phase winding when a terminal SC through 3-phase inverter is applied on the faulted 3-phase set as the mitigation measure.

Because of the mutual coupling between the two healthy 3-phase sets and one faulty 3-phase set, it has been shown in [15] that when the SC turn is located in the trailing coil of phase B in slots B2 and B4, the resultant SC current and copper loss are the largest. Fig. 1 (a) shows the positions of one turn SC fault which are marked by the two black quadrangles. Without loss of generality, all insulation faults considered in this paper are assumed in phase B and thus the terminal SC will be applied to 3-phase set ABC.

The temperature class of the polyester enameled wire is 220°C and the cut-through temperature, at which complete and irreversible damage to insulation will take place, is 320°C. At this temperature, the insulating film on the wire deforms almost instantly and sufficiently so that very low resistant electrical contact between turns will take place [16]. Thus, we can assume that after reaching the cut-through temperature, the electrical insulation resistance decreases to zero very quickly and irreversibly.

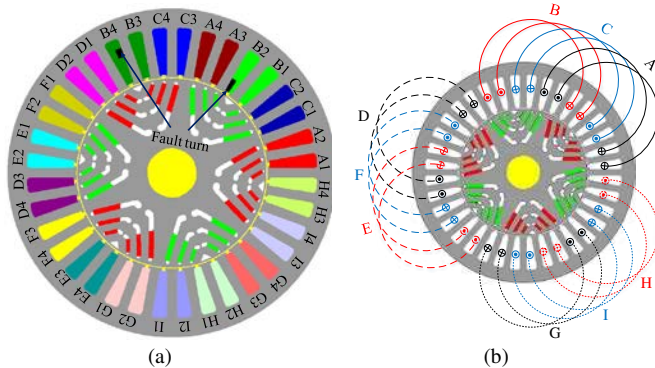


Fig. 1. Cross section of a triple redundant, 9-phase PMASynRM. (a) Named slots and short-circuit turn. (b) Layout of windings.

B. EM behavior

When turn-to-turn insulation deteriorates, the electrical resistance of the insulation reduces. Consequently, under the influence of turn-to-turn voltage, significant current may flow through the insulation. Without loss of generality, the EM

behaviors when insulation associated with one turn, two turns, three or any number of turns and one phase deteriorate in the PMASynRM can be comprehensively analyzed. Fig. 2 illustrates the electric circuit of the finite element model of the machine used in the analysis. The insulation deterioration is represented by an insulation resistance denoted by R_{in} across the associated number of turns considered. All analyses are performed at the rated condition of 4000rpm with 120A current in the healthy phases for maximum torque per Ampere (MTPA) operation. To represent a gradual process of the insulation degradation in the analyses, the insulation resistance R_{in} that forms the fault current path is varied from a quite large value (1000Ω) representing significant deterioration to a very small value (0.01mΩ) close to ideal SC.

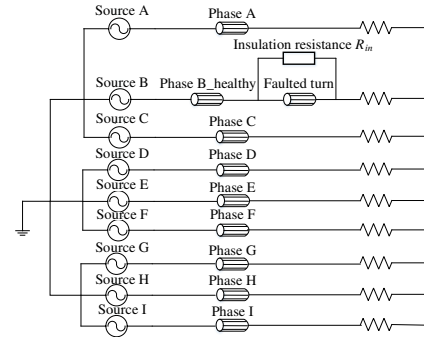


Fig. 2. The electric circuit under insulation deterioration leading to one turn, two turns, three turns SC.

It can be seen from Fig. 3 and Fig. 4 that the variations of the RMS currents in the faulted turns and insulation resistance are similar under insulation deterioration leading to SC fault. All the RMS currents reach peak when the resistance is 0.01mΩ and the peak current decreases with the number of faulted turns. However, for a given number of faulted turns, the current incurred in the faulted turns reaches a minimum lower than that in the healthy operation for a specific value of the insulation resistance as shown in Fig. 3. This is because at such a specific condition, more current is diverted into the insulation resistance branch and, consequently, the current in the faulted turns is lower than that in the healthy operation.

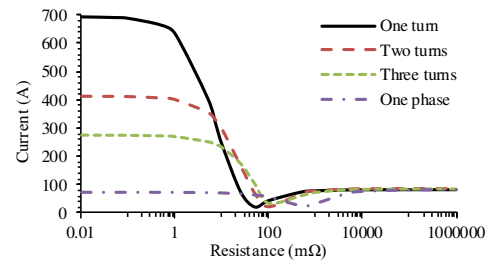


Fig. 3. RMS currents in the faulted turns under insulation deterioration.

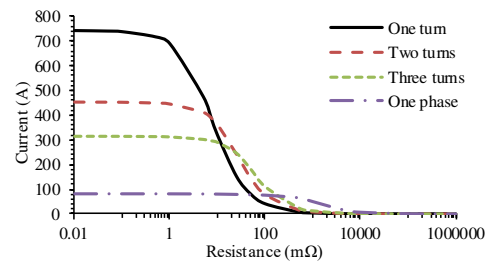


Fig. 4. RMS currents in the insulation resistance, R_{in} , under insulation deterioration.

It can be seen from Fig. 5 that all the copper losses in the faulted turns reach peak when the insulation resistance is the lowest $0.01\text{m}\Omega$ close to ideal SC. The peak loss decreases with the number of faulted turns. These results support the conclusion in [4] that under ideal SC faults, one turn SC is the most severe fault while one phase SC is thermally sustainable for this machine because the copper loss under ideal one phase SC is even lower than that under the rated healthy condition. Moreover, when the current in the faulted turns reaches a minimum, the loss in the faulted turns also reaches a minimum lower than that in the healthy operation for a specific value of the insulation resistance.

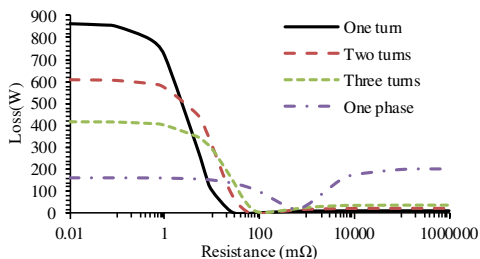


Fig. 5. Copper loss in the faulted turns under insulation deterioration.

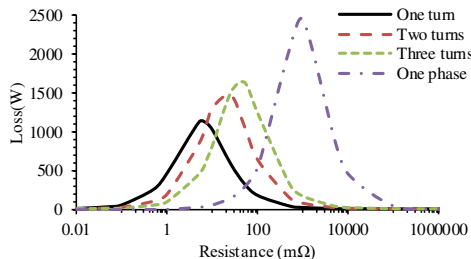


Fig. 6. Loss in the insulation resistance under insulation deterioration.

In contrast, as can be seen from Fig. 6, the losses in the insulation resistance exhibit a very different characteristic. The losses are negligible when the resistance is either very large 1000Ω , representing the early stage of insulation degradation or very small $0.01\text{m}\Omega$, close an ideal SC. When the resistance reduces from 1000Ω , the loss associated with a given number of faulted turns increases dramatically and reaches a peak which is much larger than the copper loss in ideal SC. It is evident that the peak loss increases with the number of faulted turns and hence the fault across one phase winding gives rise to the largest peak loss. This is because the resistance at which the peak occurs increases with the number of turns. However, since the probability of turn-to-turn SC fault is much larger than the other fault conditions, turn-to-turn insulation deterioration leading to SC faults is studied in this paper to assess this kind of fault behaviors.

Since the peak loss in the insulation resistance occurs before an ideal SC, fault detection and mitigation measures have to be applied when the resistance is sufficiently large to avoid that the temperature in the fault region reaches the cut-through temperature when irreversible damage or even catastrophic failure may occur.

C. Critical electrical insulation resistances

During the insulation degradation process, the actual insulation resistance is not known. However, from the

foregoing analysis two critical electrical insulation resistances are defined. As shown in Fig. 7, the insulation resistance that yields the peak loss for a given number of faulted turns is defined as the peak loss resistance denoted by R_{pmax} . For one turn fault this value is $5\text{m}\Omega$. The second critical resistance defined is the cut-through resistance R_{ct} which results in the temperature in the insulation to reach the cut-through temperature due to the loss P_{ct} incurred in it. This loss is defined as cut-through loss. From Fig. 7, for a given cut-through loss there are two corresponding electrical resistances and the larger one is the cut-through resistance as indicated.

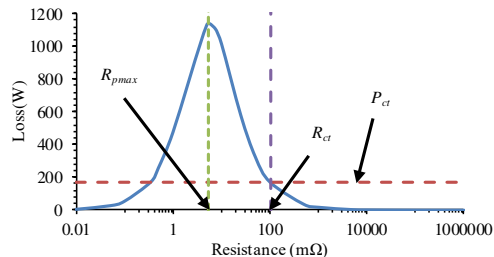


Fig. 7. Loss variation with insulation resistance under turn-to-turn insulation deterioration leading to SC fault.

The cut-through resistance R_{ct} is dependent on weakened insulation volume and the number of turns associated the weak insulation. For each condition, the fault detection and mitigation action should ideally be applied before the insulation deteriorates to reach the cut-through resistance, otherwise the electrical insulation resistance will decrease in an avalanche manner to reach the peak loss resistance, leading to complete failure. This process will be studied in section V.

III. THERMAL MODEL AND CUT THROUGH RESISTANCES

From previous analysis, if all the information of the region where insulation has significantly been deteriorated is known, a 3D thermal model representing the insulation and machine operating condition can be built to assess the resultant thermal behavior. The loss in the faulty region can be varied and the value that results in the hotspot temperature of 320°C is the cut-through loss. The corresponding cut-through resistance can be obtained according to Fig. 7 in the case of single turn SC.

However, the difficulty of this approach is that the location, shape and volume of the deteriorated insulation are often unknown. Parametric study together with appropriate assumptions is made to overcome this difficulty.

A. 3D thermal model

A 3D thermal model has been built in JMag [17] to help determine the cut-through resistance. All the thermal parameters, including conductivity, convective coefficients, heat capacity, losses and temperature boundary are set based on [7, 18]. Moreover, in [7], the 3D thermal model has been validated by tests.

The one third model of the machine with full axial length is shown in Fig. 8 with different components indicated. Fig. 9 illustrates the red region where insulation has been significantly degraded with three dimensional parameters, the length a , the thickness b and the height c . It is located close to the slot

opening and at the top of B2 coil end winding part because it is the region with the hottest temperature. The shape of weakened insulation is assumed to be cuboid. The conductivity and heat capacity of the insulation region are obtained from the insulation material, while the thermal parameters of windings are obtained by calculating the equivalent conductivity and heat capacity which consist of copper and insulation as described in [7].

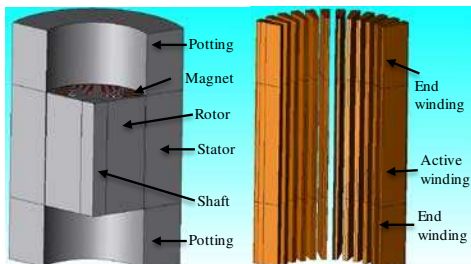


Fig. 8. One third model with whole axial length.

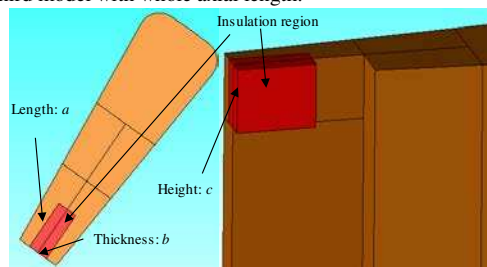


Fig. 9. Faulty insulation region in red located in one slot with three designated dimensions.

While the volume of the degraded insulation is difficult to measure in test or predict by theory, the boundaries of the three-dimensional parameters can be defined. The minimum value of the three dimensions of the insulation volume is all set to 0.1mm according to the standard of the copper wire diameter based on IEC 60317-0-1. The upper-bound of c is the half length of a turn, 224mm. If we assume each turn occupies the same volume, the upper-bound of a is 8.3mm while the maximum value for b is 2mm, equal to the slot width minus integer multiple of the wire diameter.

B. Boundary of cut-through resistance

As there are infinite possible combinations of degraded insulation volumes, two insulation volumes which result in the smallest and the largest cut-through resistance will be analyzed. Thus, the cut-through resistances of all other insulation volumes are between the two extremes.

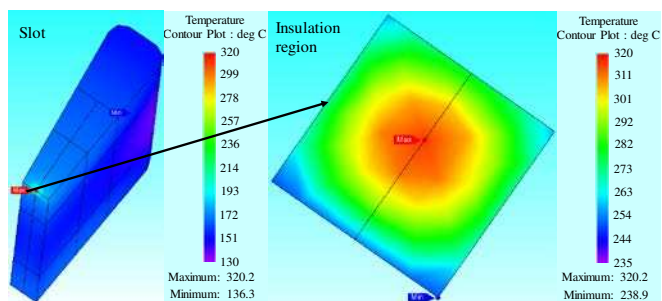


Fig. 10. Temperature distributions of slot and insulation region in Case 1.

It is likely that insulation deterioration begins in a very tiny volume. Hence Case 1 with $a=b=c=0.1\text{mm}$ is the smallest volume under consideration. It can be shown that the cut-through loss associated with Case 1 is the smallest in all other possible volumes of the dimensional combinations due to the highest heat flux density for a given loss. The cut-through loss can be determined by varying the loss in this volume under the rated operating condition, and evaluate the resultant temperature. For example, from the temperature distribution obtained from 3D thermal model as shown in Fig. 10, the average and the hotspot temperatures of the insulation region are 271°C and 320°C which reaches the cut-through temperature. Thus, the loss used under this condition is found to be the cut-through loss of Case 1 which is 1.44W ($P_{ct1,s}$). Then, according to Fig. 7, the corresponding cut-through resistance is the largest which is 13Ω ($R_{ct1,l}$).

Conversely, the largest insulation volume ($a=8.3\text{mm}$, $b=2\text{mm}$, $c=224\text{mm}$) has also been investigated. However, as the heat is mainly transferred in the b direction, when the insulation volume is sufficiently large, the thickness b instead of heat density is the most critical parameter that determines the resultant temperature. From Table I, it can be seen that for a given loss, the most optimistic case for the lowest hotspot temperature is that the thickness b is minimum and the other two parameters are at their maximum values.

TABLE I
TEMPERATURES WITH DIFFERENT THICKNESSES

Thickness b (mm)	0.1	0.5	1	2
Hotspot temperature ($^\circ\text{C}$)	328	349	375	427
Average temperature ($^\circ\text{C}$)	300	311	322	339

Thus, Case 2 ($a=8.3\text{mm}$, $b=0.1\text{mm}$, $c=224\text{mm}$) can accommodate the largest cut-through loss $P_{ct2,l}$ (144W) in which the resulted average temperature and the hotspot temperature of the insulation is 300°C and 328°C , respectively, as shown in Fig. 11. This leads to the smallest cut-through resistance $R_{ct2,s}$ (0.12Ω). The cut-through resistances of all other insulation volumes will be between 13Ω and 0.12Ω . Case 1 is the worst case which is quite likely in reality while Case 2 is the most optimistic case.

It should be noted that the same process can be used to determine the maximum and minimum cut-through resistances for any given number of turns associated with the degraded insulation volumes.

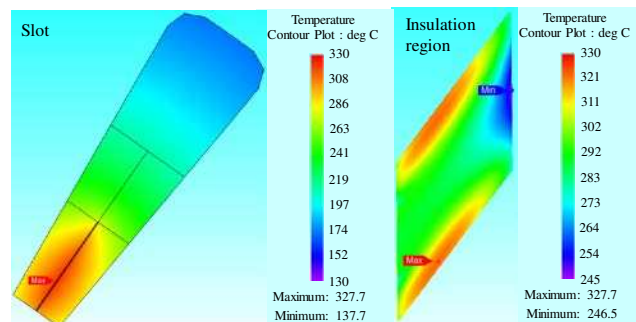


Fig. 11. Temperature distributions of slot and insulation region in Case 2.

IV. FAULT DETECTION THRESHOLD

Since the fault current and resultant heating effect are critically dependent on the insulation resistance, it is important to establish some threshold values for the resistance so that a detection scheme should be able to detect the fault and a mitigation measure is taken to prevent further deterioration.

For this purpose, simulations are performed for four typical insulation resistances: 0 (ideal SC), the peak loss value of R_{pmax} , and the maximum and minimum cut-through resistances with and without application of the mitigation measure (3-phase terminal SC). The resultant losses are presented in Table II. R_{ct1_l} , which is the maximum cut-through resistance, is also the minimum threshold of the turn-to-turn insulation resistance that a detection scheme should respond and a mitigation action applies to avoid permanent damage on insulation.

It can be seen from the Table II that the fault losses under all the cases reduce significantly after the mitigation measure. The most significant loss reduction is seen when the insulation resistance equals to the peak loss resistance. The temperature distributions when the fault is detected at three typical stages of insulation degradation and the mitigation action is subsequently taken are further analyzed.

TABLE II
LOSSES BEFORE AND AFTER MITIGATION MEASURE.

Insulation resistance (Ω)	Loss without mitigation (W)		Loss with mitigation (W)	
	Faulted turn	Insulation resistance	Faulted turn	Insulation resistance
0	837	0	126	0
0.005 (R_{pmax})	280	1136	40	46
0.12 (R_{ct2_s})	5	144	9	5
13 (R_{ct1_l})	12	1.44	9	0.05

A. Fault detected and mitigated when $R_{in} > R_{ct1_l}$

If the insulation degradation fault can be detected and the mitigation measured is applied before the insulation resistance is reduced to R_{ct1_l} (13Ω), the temperature in all possible insulation volumes will not reach the cut-through temperature and will be significantly lower after the mitigation action. The temperature distributions under one turn SC with insulation resistance of 13Ω when the mitigation action is applied and under the ideal one turn SC with the same mitigation action are shown in Fig. 12 and Fig. 13, respectively, with the same range of temperature scaling. In addition, the steady-state temperatures of various components under these two fault conditions are also compared in Table III.

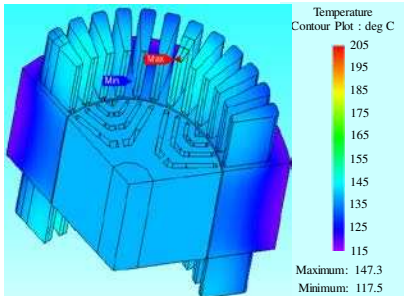


Fig. 12. Temperature distribution when insulation resistance is 13Ω and mitigation action is applied.

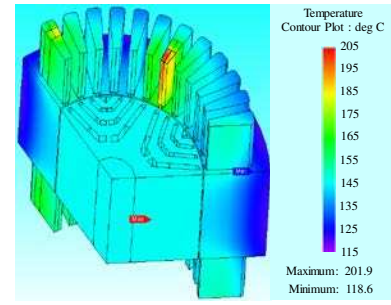


Fig. 13. Temperature distribution when insulation resistance is 0Ω and mitigation action is applied.

As observed, the average temperatures of the faulted turn and insulation as well as the hotspot temperature under one turn SC with insulation resistance of 13Ω after the mitigation measure are 41°C , 47°C and 54°C lower than those under the ideal one turn SC, respectively. The hotspot temperature of Fig. 12 is significantly lower than the permissible temperature 220°C .

TABLE III
TEMPERATURE DISTRIBUTIONS UNDER FAULT CONDITIONS WITH TWO INSULATION RESISTANCES.

Temperature ($^\circ\text{C}$)	Phase A	Phase C	Phase B_healthy	Faulted turn	Insulation	Hotspot
0Ω	140	140	151	182	194	201
13Ω	133	137	139	141	147	147
Difference	7	3	12	41	47	54

B. Fault detected and mitigated when $R_{ct1_l} \geq R_{in} \geq R_{ct2_s}$

If the insulation resistance is lower than the maximum cut-through resistance R_{ct1_l} , whether the fault insulation region will reach the cut-through temperature will depend on its volume. If the fault is detected and the mitigation measure is taken, it is likely that further deterioration can be managed because the fault current is significantly reduced. If the insulation resistance is reduced close to the minimum cut-through resistance R_{ct2_s} (0.12Ω) and no mitigation action is taken, the maximum temperature of all possible insulation volumes will reach the cut-through temperature. Consequently, the rate of reduction of the insulation resistance will accelerate, passing R_{pmax} and finally approaching zero if no mitigation is taken. However, if a mitigation action is taken before the insulation resistance reaches R_{pmax} , the resultant loss will be less than 46W as shown in Table II. Since this loss is much smaller and so is the heating effect, the mitigation action may reduce the rate of reduction or prevent further reduction of the insulation resistance, depending on the actual volume of the faulty region. In the worst case, the final steady-state temperature distribution when the mitigation action is applied but the insulation resistance is still reduced close to the ideal SC is the same as that shown in Fig. 13. Because the machine under study is designed to cope with this condition, the mitigation action is still effective in preventing a catastrophic failure and sustaining continued operation under the fault condition.

C. Fault detected and mitigated when $R_{in} \approx R_{pmax}$

When the insulation resistance approaches R_{pmax} , the resultant loss increases dramatically to more than 1000W . Thus, even if the fault is detected and the mitigation action is taken, it

is unlikely that further reduction in the insulation resistance can be stopped. However, the mitigation action is still effective in reducing the fault current when R_{in} becomes 0, and consequently facilitates fault tolerant operation.

V. TRANSIENT AGEING PROCESS

The foregoing analysis assumes a constant value of resistance for the insulation material in the faulted region. In reality, the insulation material resistivity will decrease with increase in temperature before the insulation resistance reaches the peak loss resistance and the process is irreversible. Thus, as is evident from Fig. 7, the decrease in the insulation resistance will further increase the loss and consequently the temperature. The process might trigger an avalanche effect.

The quantitative relationship between the insulation electrical resistance and the temperature is not available and may differ with different insulation materials and manufacturing processes. Thus, this paper studies an example of Case 3 in which the faulty insulation volume is assumed for $a=1\text{mm}$, $b=0.1\text{mm}$, $c=1\text{mm}$. It is also assumed that the insulation resistivity halves for every 10°C increase in temperature based on IEEE Std 43-2000 [19] to provide an insight of the transient process of insulation aging.

Electromagnetic-thermally coupled simulations introduced in [20] are performed and the results show that when the initial insulation resistances are greater than 100Ω for the assumed faulty volume the resultant fault current is very small (0.03A), and no avalanche effect is seen, i.e., insulation resistance (resistivity) reach a constant value in steady state and the hotspot temperature is below the cut-through temperature.

However, when the initial insulation resistance is 100Ω or smaller, avalanche effect will be triggered. The simulation process with initial insulation resistance of 100Ω is divided to 16 iterations, and the simulation time step is varied. In addition, the losses in the faulted turn and the insulation resistance are updated in each iteration based on the results of the EM simulation shown in Fig. 5 and Fig. 7, respectively. The detailed characteristics are introduced in [11], while the variations of insulation resistance and hotspot temperature with time are presented in Fig. 14 and Fig. 15, respectively.

As can be seen, when $t < 90\text{s}$, the insulation resistance decreases gradually but is still larger than 20Ω . Thus, the current and loss in the insulation resistance as well as the average and hotspot temperatures in the faulty insulation increase gradually with time but the hotspot temperature is below 220°C at 90s . After this point, the temperature quickly increases.

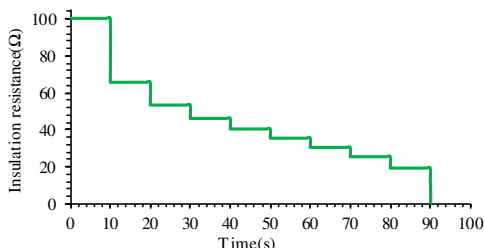


Fig. 14. Variation of insulation resistance with time.

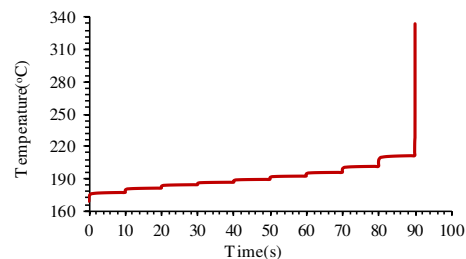


Fig. 15. Variation of hotspot temperature in faulty insulation with time.

Therefore, the insulation resistance decreases dramatically to quite small value due to the avalanche effect. The hotspot temperature exceeds 320°C in just 0.1144s.

If the insulation volume, the number of turns involved or the relationship between the insulation electrical resistance and the temperature are different from the example, the rate of insulation resistance reduction and the point of triggering the avalanche will be different but a similar trend would be seen before the insulation resistance drops down to zero. It follows that even if the insulation resistance is relatively large and the resultant loss is relatively small, a rapid deterioration may result from the fact that insulation resistance decreases with increase in temperature.

VI. TEST VALIDATION

The variation of fault current with insulation resistance across one turn is measured on the prototype machine in order to validate the electromagnetic prediction of the fault current and resultant losses. A prototype has been built and tested. The permanent magnet material is VACOMAX 225 HR, while the stator and rotor materials are 0.2mm Vacoflux 50 and Vacodur 50, respectively. The prototype PMASynRM is mounted on the test rig employing the oil cooling system as shown in Fig. 16. The machine is connected to the AVL dyno operated in speed control mode via couplings and inline torque transducer. The machine is driven by a DSP based three 3-phase inverters.

As the insulation volume and the material characteristics are hardly controllable in a test, it is not possible to experimentally validate the thermal behavior of the transient ageing process of the prototype. However, the EM behaviors under turn-to-turn insulation deterioration leading to SC fault with different insulation resistances shown in Fig. 5 and Fig. 7 are tested and validated. This validation is quite important as all the studies in this paper are based on this.

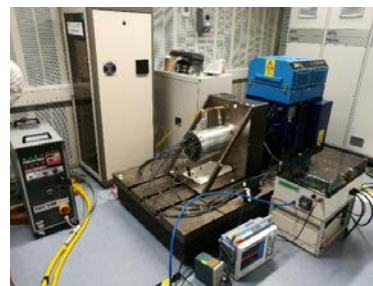


Fig. 16. Prototype on the test rig.

Two extra terminals for the turn B_f are added in phase B2 coil as shown in Fig. 17 (a) and brought out from the winding

by two thick fault-emulation cables as shown in Fig. 17 (b). The fault emulation cables are connected to extra resistor representing the state of insulation degradation via a high current relay shown in Fig. 18 and Fig. 19 to control the fault.

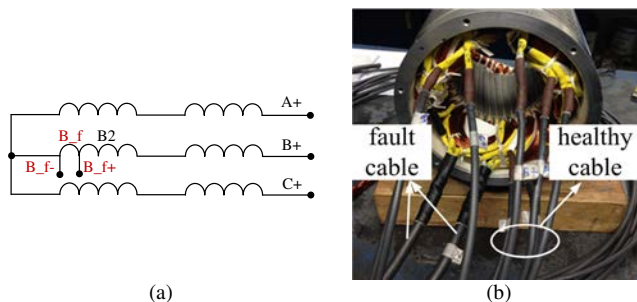


Fig. 17. Motor winding leads for turn fault. (a) The terminal connection of set ABC. (b) Leads.

Two types of resistors are used for emulation of insulation resistance. The TGHG series precision resistors [21] are used in Fig. 18 with the values of $1\text{m}\Omega$, $2\text{m}\Omega$, $5\text{m}\Omega$, $10\text{m}\Omega$, $25\text{m}\Omega$, and 0.1Ω . The copper bars with negligible resistance connect the resistor to the cable and relay. The HS aluminium housed resistors [22] are used in Fig. 19 with the values of 1Ω and 100Ω . As the resistance in this case is relatively large, cables with $2.3\text{m}\Omega$ are adopted for connection. The total resistance of the terminal cables and relay for the fault emulation is $1.4\text{m}\Omega$. Thus, single turn SC with the insulation resistance lower than $1.4\text{m}\Omega$ cannot be tested and validated.

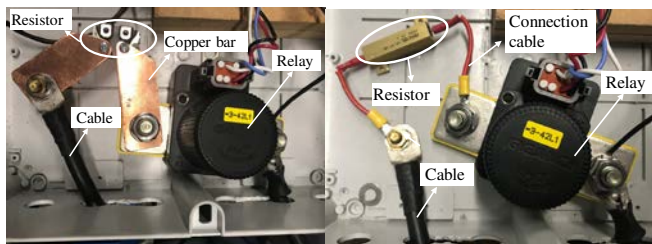


Fig. 18. Relay and precision current sense resistors.

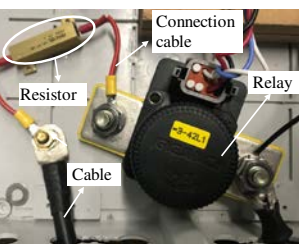


Fig. 19. Relay and aluminum housed resistors.

In order to avoid damage to the prototype, the tests are operated at 2000rpm and 1000rpm with 40A current excited in the healthy phases for MTPA operation. The results will be scaled to and compared with the prediction shown in Fig. 5 and Fig. 7. Each test will be operated for 0.2s .

A. Insulation deterioration at 2000rpm with 40A current

EM behaviors of the prototype machine under emulated turn-to-turn insulation deterioration leading to SC fault with varying insulation resistances at 2000rpm with 40A current excited in all the phases have been analyzed.

Firstly, while the predicted and measured current waveforms under the single turn SC with the minimum resistance ($1.4\text{m}\Omega$) differ slightly, the predicted RMS currents in the faulted turn and in the insulation resistance are important for thermal analysis. They differ from the measured values by 2.5% and 4.0% , respectively.

When the resistance across the emulated fault turn is varied the measured RMS currents in the faulted turn and in the insulation resistance are compared with the predicted currents

in Fig. 20. As observed, the measured and predicted currents agree quite well and the maximum differences of the RMS currents in the faulted turn and in the insulation resistance when the emulated insulation resistance varies from $1.4\text{m}\Omega$ to 100Ω are 6.3% and 4.7% , respectively.

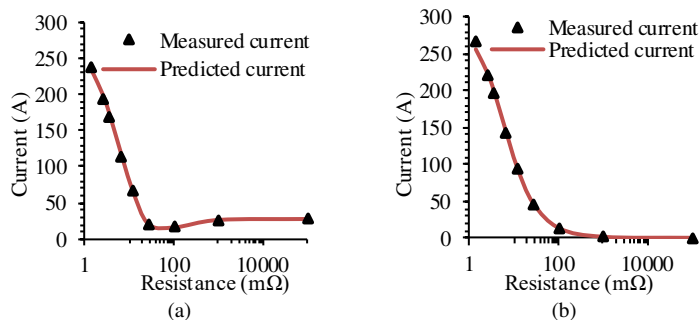


Fig. 20. Comparison of predicted and measured RMS currents under insulation deterioration at 2000rpm with 40A . (a) RMS currents in the faulted turn. (b) RMS currents in the insulation resistance.

The comparison of the predicted and measured loss variations in the faulted turn and the insulation resistance are illustrated in Fig. 21. It is evident that the measured losses match well with the predicted losses. The maximum differences of the losses in the faulted turn and the insulation resistance are 13.1% and 9.4% , respectively.

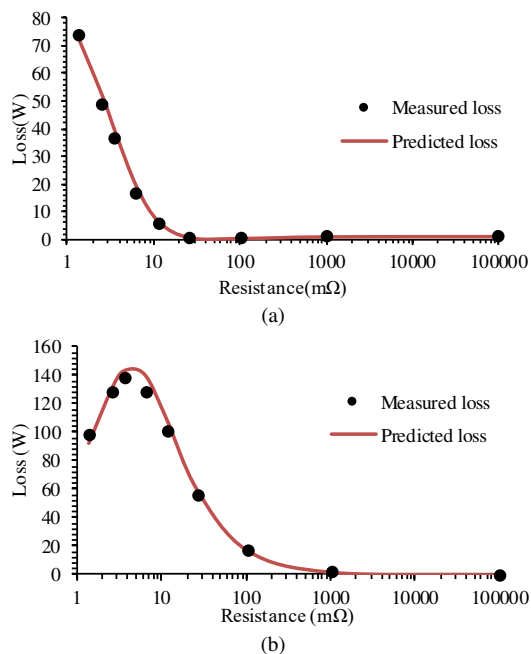


Fig. 21. Comparison of predicted and measured losses under insulation deterioration at 2000rpm with 40A . (a) Losses in the faulted turn. (b) Losses in the insulation resistance.

B. Insulation deterioration at 1000rpm with 40A current

The test was repeated at 1000rpm with 40A current excited in all the phases. From Fig. 22, the maximum differences between the predicted and measured RMS currents in the faulted turn and in the insulation resistance when the emulated insulation resistance varies from $1.4\text{m}\Omega$ to $100\text{m}\Omega$ are 15.2% and 8.6% , respectively. Therefore, the maximum differences between the predicted and measured losses in the faulted turn

and in the insulation resistance shown in Fig. 23 are relatively large, being 28.0% and 16.4%, respectively. They occur when the insulation resistance is below $5\text{m}\Omega$, and may be due to unquantified parasitic resistance of the cable and connectors. However, the predicted and measured losses in the faulted turn and in the insulation resistance have the similar trends.

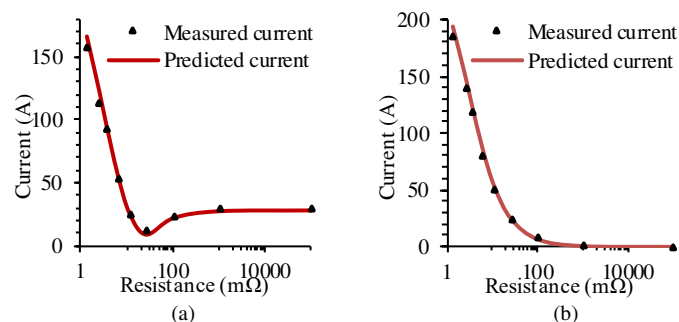


Fig. 22. Comparison of predicted and measured RMS currents under insulation deterioration at 1000rpm with 40A. (a) RMS currents in the faulted turn. (b) RMS currents in the insulation resistance.

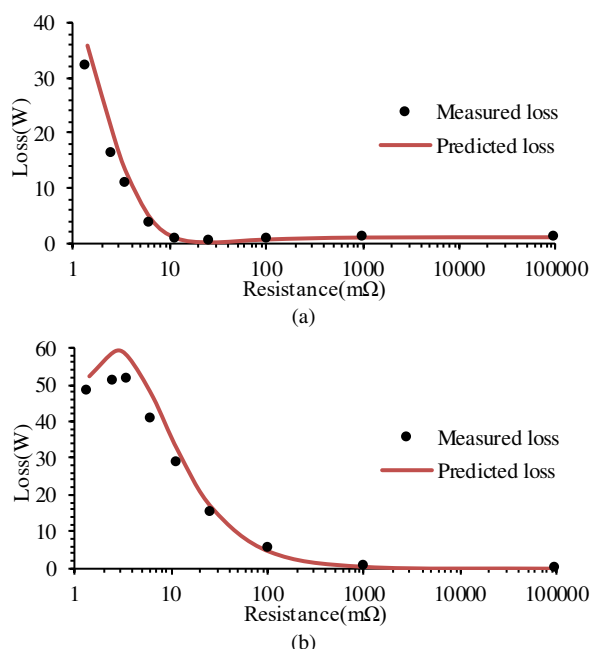


Fig. 23. Comparison of predicted and measured losses under insulation deterioration at 1000rpm with 40A. (a) Losses in the faulted turn. (b) Losses in the insulation resistance.

Therefore, the overall good matches between the measured and predicted results validate that the FE prediction of the EM behaviors under insulation deterioration leading to SC fault. Since the thermal model has also been validated in [7], these validations support the findings of the FE simulation studies in this paper.

VII. CONCLUSION

This paper has assessed the EM and thermal behavior of a triple-redundant PMASynRM under insulation deterioration leading to SC faults. It has been shown that the loss in the faulty insulation region increases with reduction of insulation resistance before reaching a peak. This behavior would dramatically increase the temperature in the faulty region and accelerate the insulation deterioration, triggering an avalanche

effect when the insulation material resistivity decreases with the increase in temperature. To prevent this process, fault detection needs to be effective when the insulation resistance is greater than a threshold and a mitigation action is taken. Finally, the tests on a prototype machine drive have validated the predicted EM behavior under turn-to-turn insulation deterioration leading to SC faults.

REFERENCES

- [1] P. O. Donnell, C. Heising, C. Singh, and S. J. Wells, "Report of Large Motor Reliability Survey of Industrial and Commercial Installations: Part I," *IEEE Trans. Ind. Appl.*, vol. IA-21, no. 4, pp. 853–864, 1985.
- [2] O. V. Thorsen and M. Dalva, "A Survey of Faults on Induction Motors in Offshore Oil Industry, Petrochemical Industry, Gas Terminals, and Oil Refineries," *IEEE Trans. Ind. Appl.*, vol. 31, no. 5, pp. 1186–1196, 1995.
- [3] M. Farahani, E. Gockenbach, and H. Borsi, et al, "Behavior of machine insulation systems subjected to accelerated thermal aging test," *IEEE Trans. Dielectrics and Electrical Insulation*, vol. 17, no. 5, pp. 1364–1372, Oct. 2010.
- [4] Z. Sun, J. Wang, D. Howe, and G. Jewell, "Analytical prediction of the short-circuit current in fault-tolerant permanent-magnet machines," *IEEE Trans. Ind. Electron.*, vol. 55, no. 12, pp. 4210–4217, Dec. 2008.
- [5] Bo Wang, J. Wang, A. Griffio, and B. Sen, "Stator Turn Fault Detection by Second Harmonic in Instantaneous Power for a Triple-Redundant Fault-Tolerant PM Drive," *IEEE Trans. Ind. Electron.*, vol. 65, no. 9, pp. 7279–7289, Sept. 2018.
- [6] A. Sarikhani and O. A. Mohammed, "Inter-turn fault detection in PM synchronous machines by physics-based back electromotive force estimation," *IEEE Trans. Ind. Electron.*, vol. 60, no. 8, pp. 3472–3484, Aug. 2013.
- [7] Y. Shi, J. Wang, and Bo Wang, "Transient 3D Lumped Parameter and 3D FE Thermal Models of a PMASynRM under Fault Conditions with Asymmetric Temperature Distribution," *IEEE Trans. Ind. Electron.*, in press, 2018.
- [8] C. Shaver, M. Rumbaugh, and S. Cain, "Accelerated thermal life testing for random-wound, polyimide wrapped medium voltage machines," *2014 IEEE Electrical Insulation Conference. EIC 2014*.
- [9] F. Kielmann and M. Kaufhold, "Evaluation analysis of thermal ageing in insulation systems of electrical machines - a historical review -," *IEEE Trans. on Dielectrics and Electrical Insulation*, vol. 17, no. 5, pp. 1373–1377, Oct. 2010.
- [10] C. M. Stephens, "Fault detection and management system for fault tolerant switched reluctance motor drives," *IEEE Trans. Ind. Appl.*, vol. 27, no. 6, pp. 1098–1102, 1991.
- [11] Y. Shi, J. Wang, R. Hu, and B. Wang, "Electromagnetic and thermal behavior of a triple redundant 9-phase PMASynRM with insulation deterioration fault," *2019 IEEE Energy Convers. Congr. Expo. ECCE 2019*, pp. 3053–3060, Baltimore, MD, USA, 2019.
- [12] Bo Wang, J. Wang, and B. Sen, et al, "A Fault-Tolerant Machine Drive Based on Permanent Magnet-Assisted Synchronous Reluctance Machine," *IEEE Trans. Ind. Appl.*, vol. 54, no. 2, pp. 1349–1359, Mar./Apr. 2018.
- [13] Bo Wang, J. Wang, A. Griffio and Y. Shi, "Investigation into Fault Tolerant Capability of a Triple Redundant PMA SynRM Drive," *IEEE Trans. Power Electron.*, vol. 34, no. 2, pp. 1611–1621, 2019.
- [14] Y. Shi and J. Wang, "Continuous demagnetization assessment for triple redundant nine-phase fault-tolerant permanent magnet machine," *J. Eng.*, vol. 2019, no. 17, pp. 4359–4363, Jun. 2019.
- [15] Y. Shi, J. Wang, and B. Wang, "Performance assessment of triple redundant nine-phase delta- and wye-connected permanent magnet-assisted synchronous reluctance motor under healthy and fault conditions," *J. Eng.*, vol. 2019, no. 17, pp. 3563–3567, Jun. 2019.
- [16] PAR UK Ltd, "POLYESTER C200 ROUND + HEAT SEALED PET FILM," datasheet.
- [17] JMAG. [Online]. Available: www.jmag-international.com.
- [18] A. Boglietti, A. Cavagnino and D. Staton, et al. " Evolution and modern approaches for thermal analysis of electrical machines," *IEEE Trans. Ind. Electron.*, vol. 56, no. 3, pp. 871–882, Mar. 2009.
- [19] IEEE Std 43-2000: "IEEE Recommended Practice for Testing Insulation Resistance of Rotating Machinery" was released on March 24, 2000.

- [20] Y. Shi, J. Wang, and B. Wang, "Electromagnetic-thermal Coupled Simulation under Various Fault Conditions of a Triple Redundant 9-phase PMASynRM," *IEEE Trans. Ind. Appl.*, vol. 56, no. 1, pp. 128-137, 2020.
- [21] Ohmite Mfg Co, "TGHG Series Precision Current Sense Resistors," datasheet.
- [22] ArcoI UK Ltd, "HS Aluminium Housed Resistors," datasheet.